Magnetic Properties of a Layered Molecular Material Comprising Manganese Hexafluoroacetylacetonate and Nitronyl Nitroxide Radicals

Andrea Caneschi, Dante Gatteschi,* and Roberta Sessoli

Department of Chemistry, University of Florence, Florence, Italy

*Received November 4, 1992**

By reaction of $Mn(hfac)_2$, hfac = hexafluoroacetylacetonate, with the NITBzald nitronyl nitroxide radical, NITBzald = 2-(4-benzaldehyde)-4,4,5,5-tetramethylimidazoline-1-oxyl 3-oxide, a compound of formula $[Mn(hfac)_2]_3(NITBzald)_2 \cdot 0.5CHCl_3$ was synthesized which was found to crystallize in the monoclinic $P2_1/n$ space group with $a = 11.277(8)$ Å, $b = 14.07(1)$ Å, $c = 26.44(2)$ Å, $\beta = 95.88(6)°$, and $Z = 2$. The structure consists of chains in which the $Mn(hfac)_2$ units are bridged by the nitronyl nitroxide radicals through the two oxygen atoms of the NO groups. The chains are connected by another $Mn(hfac)_2$ unit which is coordinated by the aldehyde oxygens of two NITBzald radicals belonging to different chains, in such a way that planes parallel to the [201] crystallographic plane are formed. The magnetic susceptibility shows a marked increase of the χT product on decreasing temperature, which can satisfactorily be reproduced by assuming that the $S = {}^5/_2$ spins of the manganese atoms within chains and $S = {}^1/_2$ spins of the radicals are strongly coupled, $J = 255$ cm^{-1} with the $H = JS_1 \cdot S_2$ Hamiltonian, while the spins of the manganese atoms bridging the chains are considered uncorrelated. The low value for the upper limit of the exchange interaction between chains through the benzaldehyde oxygen, 0.01 cm^{-1}, suggested by the EPR spectra is in agreement with the observed critical temperature to reach 3-D ferromagnetic order, $T_c = 6.4$ K, which is in the same range of T_c observed for previously reported 1-D Mn–NITR compounds. A small hysteresis was detected below T_c with a coercive field $H_c = 22$ Oe at 2 K.

Introduction

In the field of molecular magnetic materials[1,2] important results have been obtained by using stable organic radicals and magnetic metal ions.[3,4] In particular manganese(II) hexafluoroacetylacetonates, $Mn(hfac)_2$, and nitronyl nitroxides, NITR, are known to form one-dimensional compounds, $Mn(hfac)_2$–NITR, which order magnetically below 10 K.[5,7] The low critical temperature to magnetic order in these compounds is the result of compromise between the strong coupling between the spins of the metal ions and the radical within the chain, typically of the order of 10^2 cm^{-1}, and the vanishingly small exchange interactions between chains.[8] Therefore, in order to increase the critical temperatures it is necessary to induce stronger interactions between chains by finding efficient exchange pathways between them.

In order to achieve this goal we use substituent groups R on the nitronyl nitroxides which contain donor atoms in addition to the two NO groups of the radical, which can in principle connect different chains, giving rise to two- or hopefully three-dimensional structures. Whether the increase in structural complexity corresponds to an increase in the critical temperatures remains an open question, subject to the effectiveness of the branching groups in transmitting the exchange interaction. For instance when R = pyridine, a compound of formula $[Mn(hfac)_2]_3(NITpPy)_2$ was obtained,[9] which probably has a ladder structure. Even if the chains are structurally connected the critical temperatures do not increase compared to those of isolated chains.

By using the nitronyl nitroxide NITBzald, we have now synthesized $[Mn(hfac)_2]_3(NITBzald)_2$, which yielded reasonably

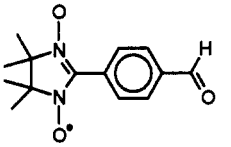

NITBzald

good single crystals, which in turn revealed a two-dimensional layered structure. We wish to report here its structure and magnetic properties, showing how also in this case the increase in structural dimensionality does not increase the critical temperature, due to the low effectiveness of the bridges connecting the chains in transmitting the exchange interaction.

Experimental Section

Synthesis. $Mn(hfac)_2$ was prepared according to the literature method.[10] NITBzald was synthesized according to the Ullman method[11] by using 1,4-dibenzaldehyde to react with 2,3-dimethyl-2,3-bis(hydroxyamino)butane in a stoichiometric ratio of 1:1. The NITBzald was separated from the other products of the reaction and purified by liquid–solid chromatography. The complex was obtained by the addition of a chloroform solution containing the radical to a heptane solution containing $Mn(hfac)_2$. Dark blue crystals of $[Mn(hfac)_2]_3(NITBzald)_2 \cdot 0.5CHCl_3$ were collected after 2 days of slow evaporation at room temperature. Anal. Calcd for $C_{58.5}F_{36}H_{40.5}Mn_3N_4O_{18}Cl_{1.5}$: C, 35.32; H, 2.05; Mn, 8.28; N, 2.82. Found: C, 36.01; H, 2.08; Mn, 8.35; N, 2.81.

X-ray Structure Determination. X-ray data were collected on a crystal of $[Mn(hfac)_2]_3(NITBzald)_2$ by using a CAD4 Enraf-Nonius four-circle diffractometer equipped with Mo Kα radiation and a graphite mono-

* Abstract published in *Advance ACS Abstracts*, August 15, 1993.

(1) *Mol. Cryst. Liq. Cryst.* **1989**, *176*.
(2) *Magnetic Molecular Materials*; Gatteschi, D., Kahn, O., Palacio, F., Eds.; NATO ASI Series E, Vol. 198; Kluwer Academic Publishers: Dordrecht, The Netherlands, 1991.
(3) Caneschi, A.; Gatteschi, D.; Rey, P. *Prog. Inorg. Chem.* **1991**, *39*, 331.
(4) Benelli, C.; Caneschi, A.; Gatteschi, D.; Sessoli, R. *Adv. Mater.* **1992**, *4*, 504.
(5) Caneschi, A.; Gatteschi, D.; Renard, J.-P.; Rey, P.; Sessoli, R. *Inorg. Chem.* **1989**, *28*, 1976.
(6) Caneschi, A.; Gatteschi, D.; Renard, J.-P.; Rey, P.; Sessoli, R. *Inorg. Chem.* **1989**, *28*, 3314.
(7) Caneschi, A.; Gatteschi, D.; Rey, P.; Sessoli, R. *Inorg. Chem.* **1991**, *30*, 3937.
(8) Ferraro, F.; Gatteschi, D.; Sessoli, R.; Corti, M. *J. Am. Chem. Soc.* **1991**, *113*, 8410.
(9) Caneschi, A.; Gatteschi, D.; Rey, P.; Sessoli, R. *Chem. Mater.* **1992**, *4*, 204.
(10) Cotton, F. A.; Holm, R. H. *J. Am. Chem. Soc.* **1960**, *86*, 2979.
(11) Ullman, E. F.; Call, L.; Osiecky, J. H. *J. Org. Chem.* **1970**, *35*, 3623. Ullman, E. F.; Osiecky, J. H.; Boocock, D. G. B.; Darcy, R. *J. Am. Chem. Soc.* **1972**, *94*, 7049.

0020-1669/93/1332-4612$04.00/0

Table I. Crystal Data and Experimental Parameters for $[Mn(hfac)_2]_3(NITBzald)_2 \cdot 0.5CHCl_3$

formula	$Mn_3C_{58.5}H_{38.5}N_4O_{18}F_{36}Cl_{1.5}$
fw	1975.5
cryst system	monoclinic
space group	$P2_1/n$
a	11.277(8) Å
b	14.07(1) Å
c	26.44(2) Å
β	95.88(6)°
V	4174 Å^3
Z	2
D(calcd)	1.572 g/cm^3
μ(Mo Kα)	5.66 cm^{-1}
temp	298 K
radiation	Mo Kα (λ = 0.710 73 Å)
refinement	R = 0.102, R_w[a] = 0.109

[a] $w = [\sigma^2(F_o) + 0.001F_o^2]^{-1}$.

chromator. The unit cell was determined by a least-squares refinement of the setting angles of 25 reflections in the range $9° < \theta < 13°$, and the space group $P2_1/n$ was uniquely determined by the systematic absences. Experimental parameters and crystallographic data are reported in Table SI (supplementary material) and in Table I in a condensed form.

The coordinates of the metal atoms were found by a Patterson map, while the other non-hydrogen atoms were revealed by successive Fourier synthesis using the SHELX76[12] package. An empirical correction for the absorption was performed.[13]

The structure solution was characterized by a large thermal motion and disorder of the CF_3 groups. For the first five CF_3 groups two sets of peaks due to the fluorine atoms were revealed by the difference Fourier synthesis and a model of disorder was introduced by assuming a rotation of the CF_3 group along the C–C bonds. The occupation factors were also refined, keeping the total constrained to unity, and found to be about 0.80–0.20 for the fluorine atoms bound to C_{18}, C_{19}, C_{23}, and C_{24} while they were found to be about 0.58–0.42 for those bound to C_{28}. Close to the inversion center not occupied by the second manganese atom other peaks were revealed by the Fourier difference map that were attributed to a disordered molecule of chloroform. The occupation factor was also refined, and it converged to a value of about 0.25; in the final refinements it was fixed to this value.

Due to the large number of parameters included in the refinement only the metal atoms, two carbon atoms of the methyl groups of the radical, and the fluorine atoms with the larger occupation factors were refined anisotropically. These atoms were chosen because they exhibit the largest anisotropy in the thermal factors.

The final full-matrix least-squares refinement converged to $R = 0.102$ and $R_w = 0.109$, and the highest peak of the last Fourier difference map, about 0.7 e/Å^3, was located close to the chloroform molecule. In spite of the high value of R the precision of the structure determination around the metal centers is not seriously affected as can be seen from the standard deviations on the positional parameters reported in Table II.

Physical Measurements. The magnetic susceptibility of a powder sample was measured using a Metronique MS03 SQUID magnetometer at a field strength of 500 Oe in the temperature range 3–50 K and 5000 Oe between 50 and 280 K. The magnetization in variable fields up to 50 kOe was measured at 3.5 K with the same instrument.

Low-field measurements were performed on a laboratory-assembled ac susceptometer based on a mutual inductance bridge measuring both the real and imaginary components of the magnetic susceptibility. The measurements were performed at 55 and 98 Hz with an alternating field of 0.5 Oe.

Hysteresis loops were recorded by applying a static magnetic field, generated by a copper solenoid immersed in liquid nitrogen, to the same ac susceptometer and successively integrating the susceptibility as a function of the static field. Due to the presence of relaxation effects the real component of the susceptibility was significantly smaller than the static susceptibility and the magnetization is therefore reported in arbitrary units.

Variable-temperature EPR spectra at X-band frequency were recorded by using a Varian E9 spectrometer equipped with an Oxford Instruments ESR9 liquid-helium continuous-flow cryostat. A crystal with dimension of about 1.2 × 0.6 × 0.4 mm was oriented by using the same diffractometer mentioned above and was found to be elongated along the a axis with the faces (011) and (0$\bar{1}\bar{1}$) largely developed. A special attachment was used in order to record the spectra by rotating the crystal about the a, b, and $c^* = a \times b$ axes.

Table II. Positional Parameters (×10^4) and Isotropic Thermal Factors (Å^2 × 10^3) for $[Mn(hfac)_2]_3(NITBzald)_2 \cdot 0.5CHCl_3$[a]

	x/a	y/b	z/c	U_{iso}[b]
Mn1	3860(1)	3334(1)	2648(1)	48(1)
Mn2	10000	5000	5000	66(2)
O1	4466(6)	7742(5)	2517(3)	57(2)
O2	4470(6)	4499(5)	2254(3)	57(2)
O3	8568(7)	5116(6)	4374(3)	77(2)
O4	2680(6)	2881(5)	1998(3)	59(2)
O5	3348(6)	1975(5)	2923(3)	61(2)
O6	2306(6)	4085(5)	2841(3)	69(2)
O7	4425(6)	3627(5)	3424(3)	58(2)
O8	8698(7)	4380(6)	5427(3)	82(2)
O9	10350(7)	3575(6)	4792(3)	81(2)
N1	4115(7)	6895(6)	2358(3)	54(2)
N2	4149(7)	5403(6)	2225(3)	53(2)
C1	4593(8)	6085(7)	2546(3)	43(2)
C2	3065(10)	6744(8)	1982(4)	66(3)
C3	3380(9)	5782(8)	1770(4)	62(3)
C4	5404(8)	5963(7)	2997(4)	48(2)
C5	6312(8)	5261(7)	3010(4)	51(3)
C6	7077(9)	5173(7)	3457(4)	55(3)
C7	6921(9)	5749(7)	3861(4)	56(3)
C8	6019(10)	6441(8)	3853(4)	67(3)
C9	5272(9)	6547(8)	3407(4)	64(3)
C10	7729(10)	5692(9)	4333(4)	70(3)
C11	1972(11)	6713(10)	2302(5)	83(4)
C12	2937(12)	7582(9)	1599(6)	104(11)
C13	2319(10)	5094(9)	1639(5)	88(9)
C14	4214(11)	5803(10)	1348(5)	87(4)
C15	1748(9)	2402(8)	2040(4)	60(3)
C16	1493(10)	1786(8)	2420(4)	68(3)
C17	2319(9)	1610(8)	2836(4)	62(3)
C18	782(11)	2535(9)	1604(5)	82(4)
C19	2009(11)	846(9)	3200(5)	84(4)
C20	1907(9)	4050(8)	3266(4)	63(3)
C21	2527(10)	3861(8)	3732(4)	73(3)
C22	3746(10)	3702(8)	3771(4)	63(3)
C23	575(11)	4257(9)	3230(5)	82(4)
C24	4382(11)	3583(9)	4303(5)	80(4)
C25	8385(11)	3560(10)	5417(5)	85(4)
C26	8845(13)	2749(11)	5173(6)	103(5)
C27	9786(12)	2879(11)	4885(5)	90(4)
C28	7308(15)	3309(13)	5769(7)	131(6)
C29	10209(19)	1997(16)	4627(8)	164(7)

[a] Standard deviations in the last digits are in parentheses. [b] $U_{iso} = {}^1/_3\sum_{ij}a_i^*a_j^*a_ia_j$.

Results

Two nonequivalent manganese atoms are present in the asymmetric unit. The first one, Mn(1) in Figure 1, is coordinated by the four oxygen of two hfac molecules and *cis* coordinated by the oxygens of the NO groups of two radicals that are related by the screw axis. Thus, chains along b are formed in which manganese atoms are bridged by NITBzald radicals as already observed in other compounds containing NITR radicals.[3-7] The second type of manganese atom, labeled Mn(2), lies on an inversion center and is octahedrally coordinated by four oxygens of two hfac molecules and two oxygens of the aldehyde substituents of two radicals. The second manganese connects adjacent chains, thus forming a plane, as shown in Figure 2, that approximately coincides with the [201] crystallographic plane.

The octahedral coordination of Mn(1) is severely distorted as can be seen in Table III where selected bond distances and angles are reported; the complete listing is available as supplementary material. The octahedron around Mn(2) is much more regular due to the lower steric hindrance. The geometry of the radical

(12) Sheldrick, G. SHELX76 System of Computing Programs. University of Cambridge, Cambridge, England, 1976. Atomic scattering factors are after: Cromer, D. T.; Lieberman, D. *J. Chem. Phys.* **1970**, *53*, 1891.
(13) Walker, N.; Stuart, D. *Acta Crystallogr.* **1983**, *A38*, 158.

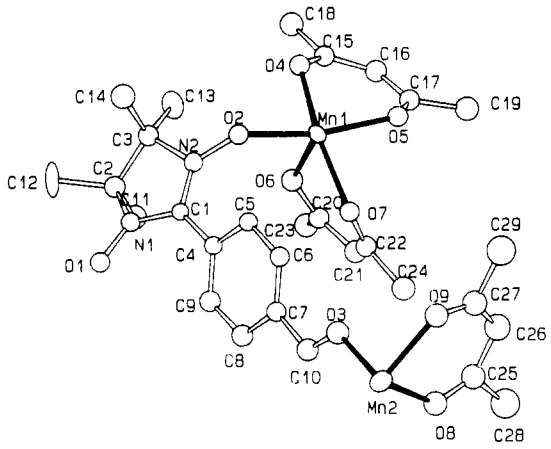

Figure 1. ORTEP view of the asymmetric unit of $[Mn(hfac)_2]_3$-$(NITBzald)_2$. The hydrogen and fluorine atoms were omitted for the sake of clarity.

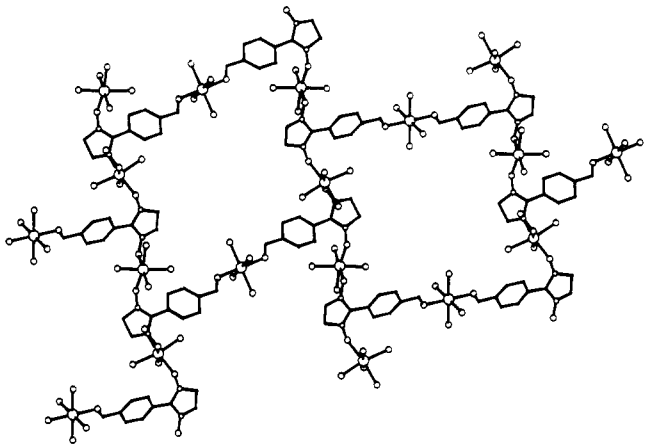

Figure 2. Schematic view of the layered structure of $[Mn(hfac)_2]_3$-$(NITBzald)_2$.

Table III. Selected Bond Distances (Å) and Angles (deg) for $[Mn(hfac)_2]_3(NITBzald)_2 \cdot 0.5CHCl_3$[a]

Mn1–O1′	2.149(7)	Mn1–O2	2.097(7)
Mn1–O4	2.158(6)	Mn1–O5	2.145(7)
Mn1–O6	2.152(7)	Mn1–O7	2.125(6)
Mn2–O3	2.197(7)	Mn2–O8	2.129(8)
Mn2–O9	2.126(8)	O1–N1	1.312(10)
O2–N2	1.322(10)	O3–C10	1.242(14)
O4–C15	1.263(12)	O5–C17	1.267(12)
O6–C20	1.254(14)	O7–C22	1.258(13)
O8–C25	1.207(16)	O9–C27	1.206(17)
N1–C1	1.334(12)	N1–C2	1.481(13)
N2–C1	1.343(12)	N2–C3	1.506(13)
C1–C4	1.437(12)	C2–C3	1.520(16)
O6–Mn1–O7	81.2(3)	O5–Mn1–O7	84.9(3)
O5–Mn1–O6	95.9(3)	O4–Mn1–O7	157.6(3)
O4–Mn1–O6	83.2(3)	O4–Mn1–O5	80.8(3)
O2–Mn1–O7	104.3(3)	O2–Mn1–O6	92.9(3)
O2–Mn1–O5	168.2(3)	O2–Mn1–O4	92.4(3)
O1′–Mn1–O7	95.1(3)	O1′–Mn1–O6	172.8(3)
O1′–Mn1–O5	89.8(3)	O1′–Mn1–O4	101.9(3)
O1′–Mn1–O2	82.0(3)	O8–Mn2–O9	84.7(3)
O3–Mn2–O9	91.0(3)	O3–Mn2–O8	86.3(3)
O9–Mn2–O8′	95.3(3)	O9–Mn2–O3′	89.0(3)
O8–Mn2–O3′	93.6(3)	Mn1–O2–N2	132.7(6)

[a] Standard deviations in the last significant digit are given in parentheses.

compares well with previous findings, and the angle formed by the mean plane of the radical and that of the phenyl ring is about 37°. In the phenyl ring the C–C bonds do not show any alternation and the C–O bond length (1.24 Å) is similar to that observed in aromatic aldehydes. The plane of the aldehyde group is almost parallel (1.9°) to that of the aromatic ring.

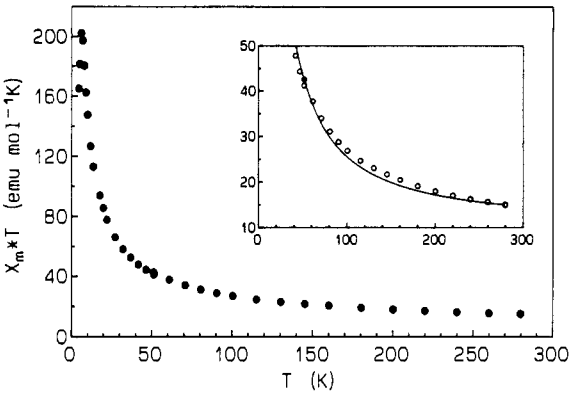

Figure 3. Temperature dependence of the product of the magnetic susceptibility with temperature. In the inset the solid line corresponds to the calculated values as described in the text.

The shortest distance between manganese atoms is within the chain (7.56 Å). Every Mn(1) has two Mn(2) atoms at 8.29 Å and another two at 9.15 Å which belong to the same plane. Within the plane the chains are well separated from each other and the shortest distance between Mn(1) atoms of adjacent chains is 16.40 Å, while the Mn(1)–Mn(1) distance between planes translated along the crystallographic *a* axis is only 11.59 Å.

The room temperature value of χT is about 15 emu K/mol, higher than the value expected for three manganese(II) ions, $S=5/2$, and two radicals, $S=1/2$, which are magnetically uncorrelated (13.875 emu K/mol for $g=2$). The χT product increases steadily on lowering the temperature reaching a maximum, $\chi T=202$ emu K/mol, at 7 K as shown in Figure 3. Below this temperature the static magnetic susceptibility remains almost constant, thus inducing a drastic decrease in the χT product. Such high values of the magnetic susceptibility clearly indicate that the exchange interaction is not limited to a finite number of spins in agreement with the extended structure observed for the compound. The magnetic moments of the manganese(II) ions are expected to be strongly antiferromagnetically coupled with the bridging radicals, and in fact the behavior observed is typical of a one-dimensional ferrimagnet. The out of chain manganese ions probably interact very weakly with the radicals.

Within this assumption the magnetic behavior at high temperature can be reproduced using the standard formula for 1-D ferrimagnets[14] adding the contribution of one uncorrelated $S=5/2$. The best fit parameters for the intrachain coupling constant is $J = 255$ cm^{-1} (we use the Hamiltonian in the form $H = JS_iS_{i+1}$), and the calculated susceptibility is reported in the inset in Figure 3. This value of J compares well with those previously observed in manganese-radical chains but is smaller than that observed when the radical has R = 4-methoxyphenyl.[7] The difference can be ascribed to the different inductive effect of the substituent of the aromatic ring.

The presence of a strong intrachain interaction may induce a magnetic phase transition even if the interaction between chains through the aldehyde is supposed to be very small. A phase transition was in fact revealed by the ac susceptibility measurements. In Figure 4 the real and imaginary components of the susceptibility in zero applied field are reported. At about 6.4 K the onset of the imaginary component of the susceptibility is observed revealing the presence of internal fields due to the magnetic ordering. The increase of χ'' is accompanied by a decrease of χ', as often observed in this kind of material for which the domain walls cannot move freely and completely follow the

(14) Seiden, J. *J. Phys. Lett. (Paris)* **1983**, *44*, L947.

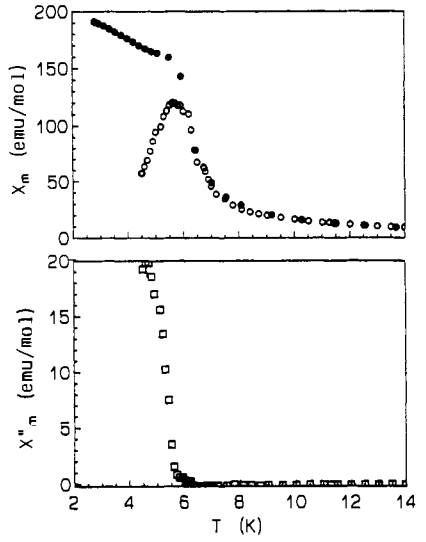

Figure 4. Real (top) and imaginary (bottom) components of the ac susceptibility at 98 Hz. The full circles represents the dc susceptibility in an external field of 50 Oe.

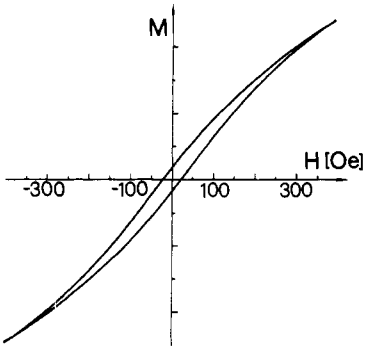

Figure 5. Hysteresis loop recorded on [Mn(hfac)$_2$]$_3$(NITBzald)$_2$ at 2 K. The magnetization is reported in arbitrary units.

oscillating field.[15] However the presence of antiferromagnetism can be excluded because the static susceptibility does not decrease below T_c as shown in Figure 4. The temperature of the maximum in χ'' remains unchanged working at different frequencies of the alternating field suggesting that we are not observing superparamagnetism or a spin-glasslike behavior.

A small hysteresis is observed, as shown in Figure 5, and the coercive field increases on lowering the temperature from about 2 Oe at 4.2 K to 22 Oe at 2 K. Since the loop was measured with an ac susceptometer, it was not possible to give an absolute value to the magnetization.

In order to gain more insight into the nature of the ordered phase we measured the magnetization as a function of the external field below the critical temperature. The results, reported in Figure 6, reveal a rapid increase of the magnetization in low magnetic field which corresponds to the presence of spontaneous magnetization. Above 2 kOe the slope of the curve decreases smoothly, but saturation is reached only above 40 kOe. The value reached at 50 kOe, $M = 12.8\ \mu_B$ per formula unit, is in good agreement with the value of 13 μ_B expected for $S_{tot.}=^{13}/_2$ originated by the parallel alignment of the three spins $S=^5/_2$ of the metal ions which are antiparallel to the spin $S=^1/_2$ of the radicals.

The EPR spectra of a microcrystalline powdered specimen show at room temperature a single line centered at $g = 2$ with peak to peak line width $\Delta H_{pp} = 280$ G. No transition is observed at half-field. Below 20 K a change in the structure of the signal becomes observable with components moving upfield and downfield on decreasing the temperature as shown in Figure 7. At least five absorpions are observed at the lowest temperature.

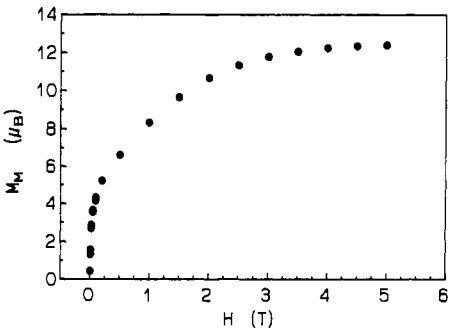

Figure 6. Magnetization curve of [Mn(hfac)$_2$]$_3$(NITBzald)$_2$ obtained at 3.5 K.

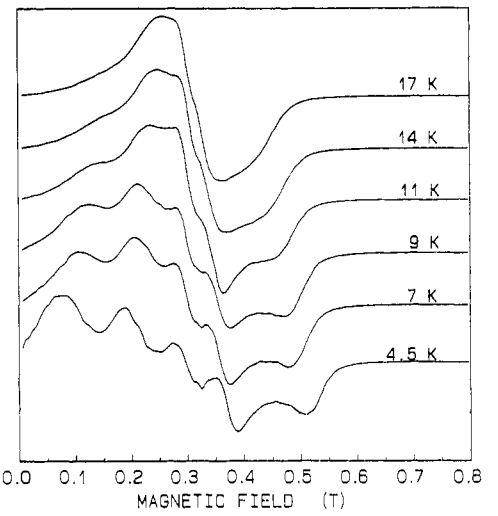

Figure 7. Temperature dependence of the EPR spectrum of a powdered specimen of [Mn(hfac)$_2$]$_3$(NITBzald)$_2$.

The analysis of the single-crystal EPR spectra is complicated by the presence at low temperature of two signals in almost every orientation which cannot always be resolved. In particular two signals are observed when the magnetic field is parallel to the *b* axis, where the absorption of the two magnetically nonequivalent sites in a monoclinic crystal should merge to one line. All the signals show a sensible shift of the resonance field on decreasing temperature.

Discussion

[Mn(hfac)$_2$]$_3$(NITBzald)$_2$ is the first example of a a two-dimensional structure comprising NITR radicals, but, in spite of it, the magnetic behavior is fully reminescent of that of one-dimensional material. The magnetic susceptibility is in fact well reproduced by using the available formulas for 1-D systems suggesting that the spin of the manganese atom is weakly interacting with the radical through the benzaldehyde group. The EPR spectra confirm this assumption. In fact the presence of two signals in every orientation can only be explained by assuming that one is associated with the chains and the other with the Mn(2) ions connecting the chains. The Mn(1) and NITR radicals are strongly coupled yielding one signal, and they are well-known to experience large *g*-shifts at low temperature, due to strong internal fields generated by the large spin correlation.[16-18] If it is assumed that the coupling between the chains and the Mn(2) ions is smaller than the difference in resonance fields,

(15) Palacio, F.; Lazaro, F. J.; van Duyneveldt, A. J. *Mol. Cryst. Liq. Cryst.* **1989**, *176*, 289.

(16) Nagata, K.; Tazuke, Y. J. *Phys. Soc. Jpn.* **1972**, *32*, 337.
(17) Richards, P. M. In *Local Properties at Phase Transitions*; Ed. Compositori: Bologna, Italy, 1973.
(18) Gatteschi, D.; Sessoli, R. *Magn. Reson. Rev.* **1990**, *15*, 1.

then the presence of two signals is justified. The upper limit for the exchange interaction between chains and Mn(2) can therefore be estimated as ca. 0.01 cm^{-1}.

Even if the spin of the manganese atoms connecting the chains is almost isolated, the *g*-shift observed in the EPR spectra suggests that it also experiences the internal field originated by the short-range correlation in the chains. By using the point dipolar approximation, we have calculated the magnetic field at the Mn(2) site generated by a parallel alignment of the manganese spins of the chains which are in turn antiparallel to those of the radicals. The amplitude and the direction of the internal field present at the Mn(2) site depends of course on the direction chosen for the spin alignment, which remains unknown due to the lack of single-crystal magnetic measurements; however, it does not exceed 300 Oe. This relatively low value can justify the unusual magnetization curve which requires a strong magnetic field to reach saturation although at low field there is evidence of spontaneous alignment of the magnetic moments.

This picture of strong correlation within chains, and very weak correlation between chains, easily explains why the critical temperature is in the same range as those previously reported for one-dimensional materials even if the lattice dimensionality is increased from one to two. In fact the dipolar interactions must essentially be responsible for the crossover from one- to three-dimensional magnetic behavior, and the distances between chains are not lower here compared to those in the previously reported Mn–NITR chains. Attempts are being made to find R groups which are able to connect the chains transmitting the exchange interaction in a more efficient way.

Acknowledgment. The financial support of the MURST and the "Progetto Finalizzato Materiali Speciali per Tecnologie Avanzate" is gratefully acknowledged.

Supplementary Material Available: Tables SI–SVI, reporting respectively crystallographic and experimental parameters, positional parameters for the fluorine and chloroform atoms, anisotropic thermal factors, complete bond lengths and angles, and least-squares planes (9 pages). Ordering information is given on any current masthead page.